Reservoir Forming Dynamics of Differential Accumulation of Tight Oil in the Yanchang Formation Chang 8 Member in the Longdong Area, Ordos Basin, Central China

Jingru Yang[1]*, Xianyang Liu[2] and Wanglin Xu[1]

[1]Research Institute of Petroleum Exploration and Development, CNPC, Beijing, China, [2]Research Institute of Petroleum Exploration and Development, Changqing Oilfield Company, CNPC, Xian, China

Tight oil is usually accumulated near source rocks after short-distance migration. For the Chang 8 member tight oil reservoir in the Longdong area of the Ordos Basin, however, the tight oil accumulation does not completely follow the source control theory, which states that richer tight oil is found in zones closer to the source rock. The causes behind such differential accumulation need to be investigated. On the basis of previous studies, this paper accurately restores the oil migration dynamics in the main reservoir-forming period by using the latest paleo-hydrodynamic restoration technology through mudstone compaction analysis. The oil migration dynamics are then compared with the start-up pressure gradient of the transport layer along the potential oil migration path during the main reservoir-forming period. Finally, combined with the paleo-structural characteristics during the main reservoir-forming period, the causes for the differential accumulation of tight oil in the Chang 8 member of the Longdong area are analyzed. The results show that: 1) during the main reservoir-forming period, tight oil in the Chang 8 member tended to and could migrate from the north and northeast to the southwest and has accumulated in the nose-like paleo-structure in the southwest; and 2) following the main reservoir-forming period, as the reservoir formation was compacted and the fluid pressure and hydrocarbon generation capacity reduced, oil accumulated nearer the source rock, and to a lesser extent than it did during the reservoir-forming period. In these two stages, changes in the intensity of oil migration dynamics dominated the differential accumulation of tight oil. This study provides a new perspective for similar efforts.

Keywords: tight oil, oil migration dynamics, start-up pressure gradient, Longdong area, Ordos Basin

INTRODUCTION

Tight oil is diversely defined (Clarkson et al., 2011; Zhao, et al., 2012; Zou et al., 2015; Du et al., 2016; Zhao et al., 2017). It is commonly recognized that tight oil is crude oil that was expelled from the source rock and accumulated in tight sandstone or carbonate rock near or within the source rocks, and that cannot flow naturally out of a well, but can only be produced with the support of stimulation techniques (e.g., horizontal well drilling and hydraulic fracturing). Tight oil accumulation can be classified into two types: continuous (Gautier et al., 1995; Schmoker, 1995; Zou et al., 2009) or

FIGURE 1 | (A) Geographic location of the Ordos Basin **(B)** Geographic location of the Longdong area in the Ordos Basin **(C)** distribution of Chang 7 high-quality source rocks[13] and the Chang 8 reservoirs.
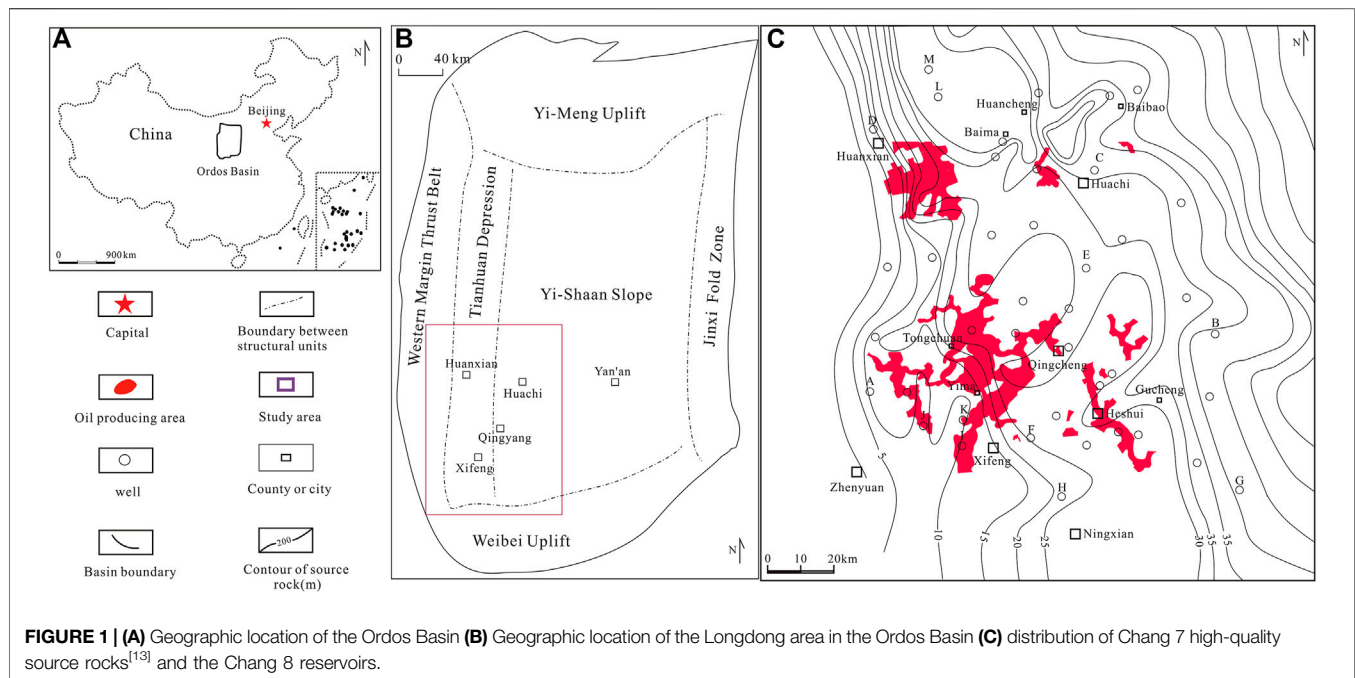
quasi-continuous (Zhao et al., 2012). Reservoir compaction and oil accumulation are often related to one another in three cases: compaction before accumulation (e.g., the Chang 8 reservoir in the Ordos Basin; Fu et al., 2017), accumulation before compaction (e.g., Yanchang Formation in the Zhenjing area of the Ordos Basin; Liu et al., 2012), and simultaneous compaction and accumulation (e.g., the Chang 7 Member in southwestern Ordos Basin; Zhao et al., 2018).

The Longdong area in southwestern Ordos Basin (**Figure 1A**) stretches over the Yi-Shaan Slope and Tianhuan Depression. The study area, a region of approximately 30,000 km^2, is bounded by Miaogou in the north, Taichang in the south, Guoyuan in the west, and Taibai in the east. The Yanchang Formation belongs to the Upper Triassic of the Mesozoic and can be divided into five members and 10 oil groups (**Figure 2**). Among the oil groups, the Chang 7 Oil Group belongs to the third member of the Yanchang Formation (T3y3), which comprises lacustrine sedimentary facies and a lithology of mainly dark-colored mudstone, carbonaceous mudstone, and fine sandstone and siltstone intercalated with oil shale, with a thickness of 80–100 m. Chang 7 serves as the main source rocks of the Yanchang Formation. The Chang 8 Oil Group, which belongs to the second member (T3y2) and is underlying Chang 7, comprises sandstones and shales of lacustrine-delta sedimentary facies, with a thickness of 170–185 m, and with the sandstones having formed the main oil reservoirs of Chang 8 (**Figure 2**). The commercial hydrocarbon reservoirs of Chang 8 were discovered in the Longdong area. Chang 8 can be subdivided into two thin layers: the Chang 8^1 and Chang 8^2 members (**Figure 2**).

Oil exploration practices have revealed the presence of oil zones in Chang 8 in the southwest part of the Longdong area, forming the Xifeng, Zhenbei, Heshui, and other oilfields with higher oil enrichment (**Figure 1B**). Further, the alternation of oil

and water zones in Chang 8 has also been identified in the north of Longdong area, forming the Huachi, Huanxian, and other oilfields with lower oil enrichment. According to the distribution of Chang 7 high-quality source rocks (Zhang et al., 2009; Li et al., 2017; Li et al., 2019; Li J. et al., 2020) and the Chang 8 oilfields (**Figure 1B**), within the high-quality source rocks, the Hushui Oilfield with rich oil reserves and the Huachi Oilfield with less-rich oil reserves have been discovered. Moreover, at the edge of the high-quality source rocks, the Xifeng Oilfield with rich oil reserves and Huanxian Oilfield with less-rich oil reserves are well developed. What caused such differential accumulation of tight oil? What are the oil migration dynamics? Many related studies have been carried out on the tight reservoirs of the Yanchang Formation to understand the other characteristics of this area. For example, the diagenesis of tight reservoirs (Xi et al., 2019a), the influence of clastic composition on the formation of tight reservoirs (Wang et al., 2020), and the genesis of calcite in tight reservoirs (Xi et al., 2019b) have all been study targets. Additional previous studies on Chang 8 in the Longdong area have suggested three stages of oil accumulation and the Late Jurassic sand bodies with good physical properties and lipophilic pores in sandstones that have developed since the Early Cretaceous as oil migration paths (Luo et al., 2010). In terms of tight oil migration and accumulation dynamics in the Longdong area, previous studies have mainly focused only the relationships between longitudinal overpressure distribution and oil production and horizontal fluid potential and oil distribution (Ying et al., 2011). There is a lack of analysis on the variation of accumulation dynamics and its coupling relationship with resistance, as well as the relationship between differential accumulation.

In this study, we restored the oil migration dynamics in the main reservoir-forming period by using the latest paleo-

FIGURE 2 | Structural contour map of the top of the Chang 8 Oil Group of the Yanchang Formation (Upper Triassic), along with the regional distribution of Triassic oil production areas and the location of the study area in the Ordos Basin (after Zhang et al., 2009).
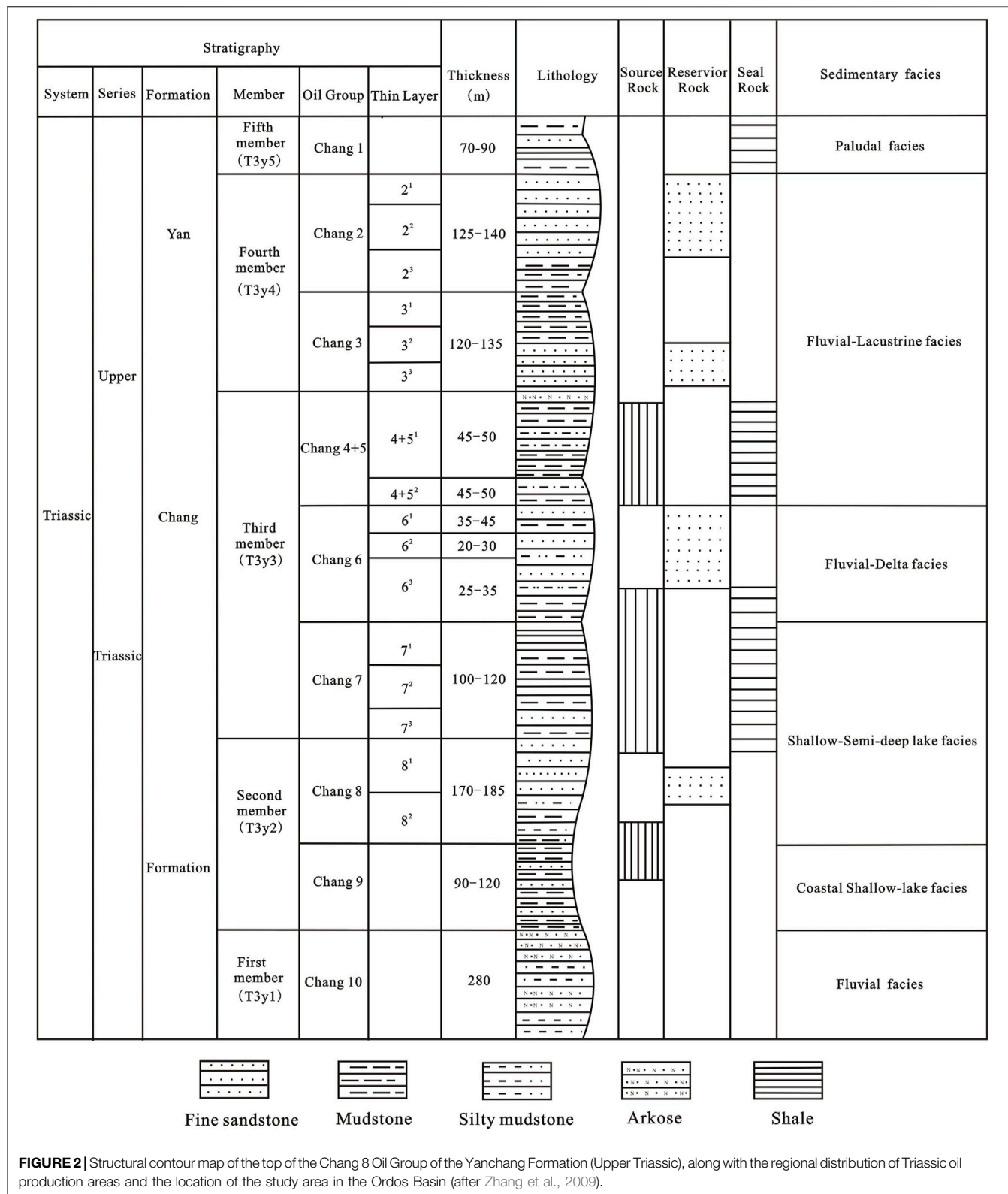
hydrodynamic restoration technology (the loading–unloading curve method) through a compaction analysis of mudstone. Start-up pressure gradient was introduced as the micro scale

of petroleum migration and accumulation in the tight reservoir. Then, we compared the oil migration dynamics with the start-up pressure gradient of the transport layer along the potential oil
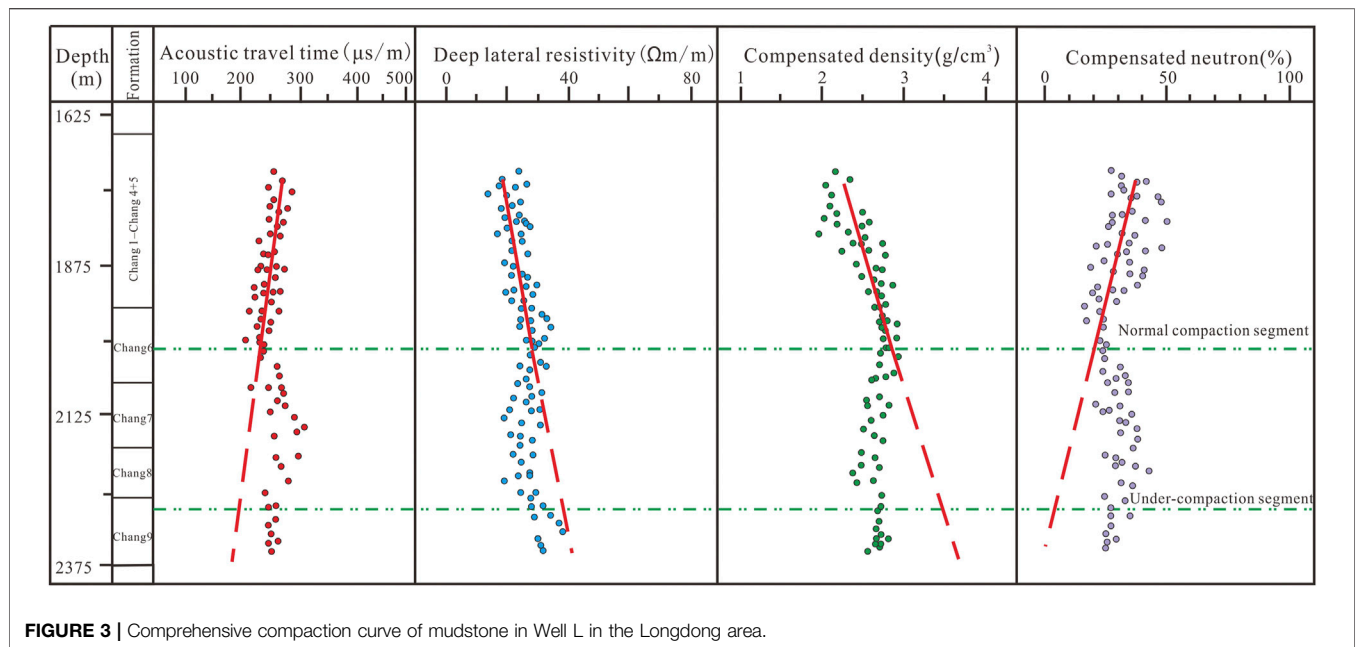
FIGURE 3 | Comprehensive compaction curve of mudstone in Well L in the Longdong area.

migration path in the main reservoir-forming period. Finally, combined with the paleo-structural characteristics in the main reservoir-forming period, we analyzed the causes for the differential accumulation of tight oil in the Chang 8 member of the Longdong area. This study is expected to provide a new perspective for similar efforts.

MUDSTONE COMPACTION ANALYSIS

Mudstone is widely used in formation compaction analysis, since it is less vulnerable to non-compaction diagenesis processes (e.g., cementation, dissolution, and metasomatism) than sandstone (Athy, 1930; Magara, 1968; Chen and Tang, 1981; Wang et al., 2003; Li et al., 2017; Fan and Wang, 2021). Further, because mudstone is more capable of overpressure retention than adjacent sandstone, mudstone overpressure can be transmitted to adjacent sandstone *via* multiple channels (e.g., hydraulic fracture), which leads to the synchronous change of pressure between the mudstone and the adjacent sandstone (Wang et al., 2005). If there is no long-distance migration path (e.g., a fracture or unconformity), the abnormal pressure in permeable sandstone generally comes from the pressure transfer of adjacent abnormally high-pressure argillaceous strata (Fertl, 1976; Magara, 1978; Osborne and Swarbrick, 1997). Therefore, mudstone is usually used to study the formation fluid pressure caused by compaction.

Data Acquisition
Acoustic travel time is subject to the effects of many factors (e.g., the borehole diameter, fractures, gas-bearing potential, and tight-zone characteristics); thus, it does not typically have a linear relationship with porosity. By comparing the acoustic qualities, as well as the resistivity, density, compensated neutrons, and other logging data from the same lithology, it can be generally confirmed to what extent

the acoustic travel time reflects the corresponding change in porosity. This method is known as the comprehensive compaction curve comparison method (Wang et al., 2003). In this study, from a pure mudstone interval, we acquired the acoustic and resistivity logging data, which reflect the rock conduction effect, as well as the density and neutron logging data, which reflect the rock volume property. These four conventional logging sequences were combined for compaction analysis.

Segmentation of Mudstone Compaction
The comprehensive compaction curve (**Figure 3**) plotted for all 10 members in the study area (Chang 1–10), shows a trend that, from Chang 1 to Chang 4 + 5, the acoustic travel time decreases, while the deep lateral resistivity increases, the formation density increases, and the neutron porosity decreases; below Chang 4 + 5, from Chang 6 to Chang 8, the acoustic travel time, resistivity, density, and neutron porosity show reverse behavior and are synchronized. Only when this synchronization occurs can the segmented compaction of mudstone be confirmed (Fertl and Timko, 1972; Hermanrud et al., 1998). Thus, it can be confirmed that Chang 1 to Chang 4 + 5 is a normal compaction segment, and Chang 6 to Chang 8 is an under-compaction segment. The normal compaction segment is usually characterized by the following equation (**Eq. 1**):

$$\Delta t = \Delta t_0 e^{-cz} \qquad (1)$$

where z is the buried depth, Δt is the acoustic travel time at the buried depth z, Δt_0 is the surface acoustic travel time, and c is the compaction slope.

Key Controlling Factors for Mudstone Compaction
The compaction process of mudstone is predominantly affected by the formation deposition rate. Generally, if the deposition rate

FIGURE 4 | Correlation between compaction slope and deposition rate for normal compaction segments in the Longdong area.
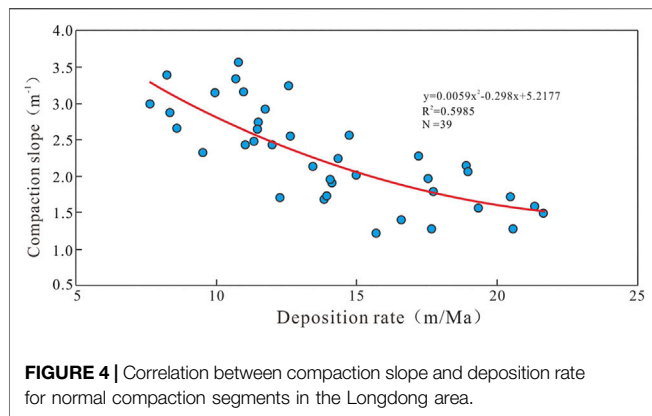
is low, the mudstone particles experience a sufficient time for achieving better (horizontal) arrangement, such that the porosity may decrease rapidly with the buried depth, resulting in a larger compaction slope. In contrast, if the deposition rate is high, the mudstone particles do not have enough time to arrange horizontally, resulting in a higher porosity at the given depth, and thereby a smaller compaction slope. As shown in **Figure 4**; **Table 1**, the deposition rate in the study area is apparently negatively correlated with the compaction slope for the normal compaction segment, that is, the higher the deposition rate, the smaller the compaction slope. In other words, for the study area, a higher deposition rate has caused unfavorable conditions for mudstone compaction. In addition, the lithologic combination, argillaceous content, and sediment source can also affect the slope of mudstone compaction.

OIL MIGRATION DYNAMICS DURING THE MAIN RESERVOIR-FORMING PERIOD
Determination of the Main Reservoir-Forming Period

Microscopic diagenetic fluid information (e.g., authigenic illite dating, carbon/oxygen isotope analysis of authigenic calcite, and fluid inclusion temperature measurement) show that the oil of Chang 8 in the Longdong area extensively accumulated mainly at the end of the Early Cretaceous, when the buried depth reached its maximum (Fan et al., 2013). The high-quality Chang 7 source rocks are considered the main source rocks of the Mesozoic in the Ordos Basin, and the study area is located within those high-quality source rocks (Zhang et al., 2009). Under the action of source–reservoir pressure differences and capillary pressure, oil first migrated from Chang 7 source rocks to the Chang 8 member. After entering the Chang 8 tight reservoir, the oil experienced a

secondary migration under the overpressure caused by under-compaction in Chang 8, in addition to the residual pressure carried from the source rock.

Method to Restore Oil Migration Dynamics During the Main Reservoir-Forming Period

The equivalent depth method (Magara, 1968) is widely used in the calculation of overpressure caused by under-compaction. For this method, essentially, an equation is established assuming that the effective stress at a point in the under-compacted interval is equal to the effective stress in the normal compaction segment with the same porosity. Then, Terzaghi's equation (Terzaghi, 1943) is used to calculate the fluid pressure and overpressure in the under-compacted interval. At the same time, based on the assumption of compaction as an irreversible process, it is considered that the current compaction curve can reflect the compaction in the period with the maximum buried depth, and thus the equivalent depth method can be used to calculate the overpressure in such a period. In fact, however, the current compaction curve can reflect the compaction pattern, but its application for abnormal pressure restoration in the period with the maximum buried depth may involve significant uncertainties. Accordingly, the occurrences of demonstrated formation resilience after intense uplifting, denudation, and unloading in the later stage need to be better determined by experiments. Many studies have reported the formation resilience after structural uplifting (Ren and Sun, 2005; Li D. et al., 2020).

Rock mechanics experiments with surface mudstone cores are difficult to implement due to the strong elasticity of such cores. We measured the porosity of seven shale samples taken at different buried depths of Chang 7 in the study area. The results show that the pore volume of shale increases with the decline of effective stress, indicating that the mudstone of the study area exhibited resilience to a certain extent during the process of structural uplifting. Also, according to the correlation between pore volume and effective stress (**Figure 5A**), the resilience of shale pores conformed to a good logarithmic relationship, with a correlation coefficient of more than 0.9. The curve was morphologically consistent with the Bowers unloading curve (Bowers, 1995). Using the slope (**Eq. 2**) obtained by fitting these data according to the linear relationship (**Figure 5B**), the pore resilience coefficient during structural uplifting could be determined as follows:

$$C_r = \frac{\Delta \phi}{\Delta \sigma} \qquad (2)$$

where C_r is the pore resilience coefficient, $\Delta \Phi$ is the change in pore volume, and $\Delta \sigma$ is the change in effective stress. It was indicated in the experiment that the faster the pressure dropped, the more the

TABLE 1 | Sedimentation rate and slope in the normal compaction section of some wells in the study area.

Well	A	B	C	D	E	F	G	H	I	J
Compaction slope (m-1)	3.00	3.41	2.89	2.67	2.34	3.16	3.58	3.35	3.26	1.73
Deposition rate (m/Ma)	7.50	8.04	8.17	8.42	9.27	9.66	10.45	10.36	12.17	13.41
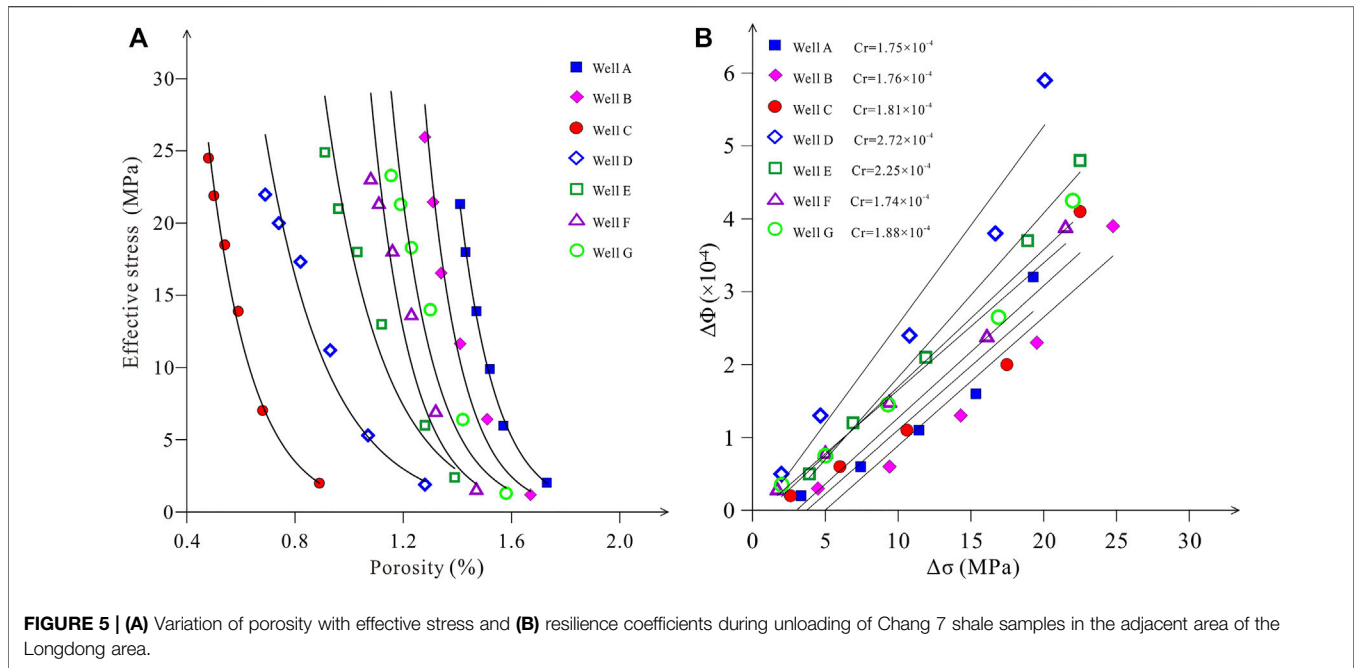
FIGURE 5 | (A) Variation of porosity with effective stress and **(B)** resilience coefficients during unloading of Chang 7 shale samples in the adjacent area of the Longdong area.
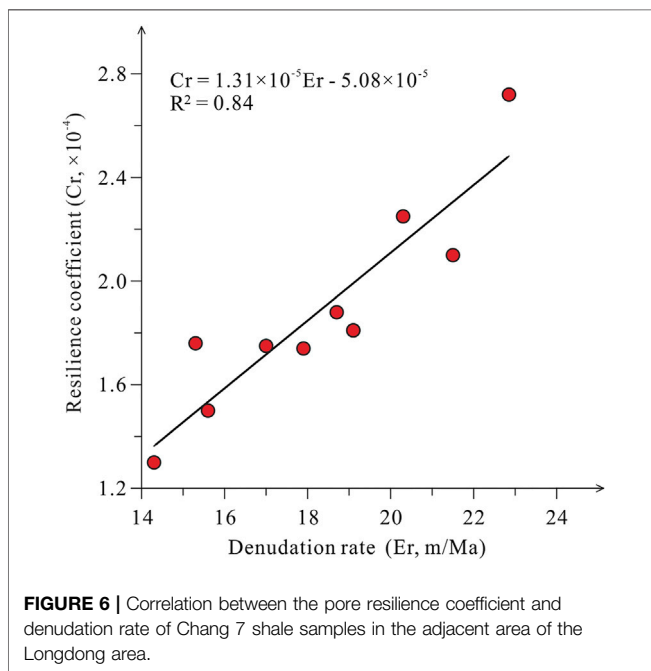
FIGURE 6 | Correlation between the pore resilience coefficient and denudation rate of Chang 7 shale samples in the adjacent area of the Longdong area.

shale pores swelled, owing to the speed of structural uplifting, which has a significant impact on shale resilience. Through the statistical analysis, the denudation rate was found to have a certain positive correlation with the resilience coefficient (**Figure 6**), with the square of correlation coefficient reaching up to 0.84. Accordingly, the resilience coefficient of Chang 8 mudstone in the untested portions of the study area could be calculated.

By using the resilience coefficient and the present-day shale porosity, the shale porosity in the period with the maximum

buried depth could be restored. According to the exponential relationship between effective stress and porosity (the loading curve) of the Bowles method (Bowers, 1995), the loading curve (**Eq. 3**; Han, 2020) was plotted using the restored mudstone porosity and effective stress for the normal compaction segment in the period with the maximum buried depth. Moreover, the unloading curve (**Eq. 4**; Han, 2020) could be plotted using the resilience coefficient and the measured present-day pressure (**Figures 7A,B**):

Loading curve:

$$\phi_b = ae^{b\sigma_b} \tag{3}$$

Unloading curve:

$$C_r = \frac{\phi_p - \phi_b}{\sigma_b - \sigma_p} \tag{4}$$

It should be noted that the porosity at the intersection of the loading curve and the unloading curve is equal (Han, 2020).

$$ae^{b\sigma_b} = \phi_p - C_r(\sigma_b - \sigma_p) \tag{5}$$

Next, the effective paleo-stress could be obtained by using the iterative method, and then, the overpressure caused by under-compaction in the period with the maximum buried depth could be calculated (**Eq. 6**; Han, 2020):

$$\Delta P_{dc} = S_b - \sigma_b - P_{wb} \tag{6}$$

where Φ_P and Φ_b are the porosity in the present day and the porosity in the period with the maximum buried depth, respectively; σ_P is the present-day effective stress; a and b are fitting constants of loading curves; C_r is the pore resilience coefficient; $\Delta\Phi$ is the resilience of porosity; $\Delta\sigma$ is the effective

FIGURE 7 | (A) The loading and unloading curves model and **(B)** loading and unloading curves of Well Z in the Longdong area.
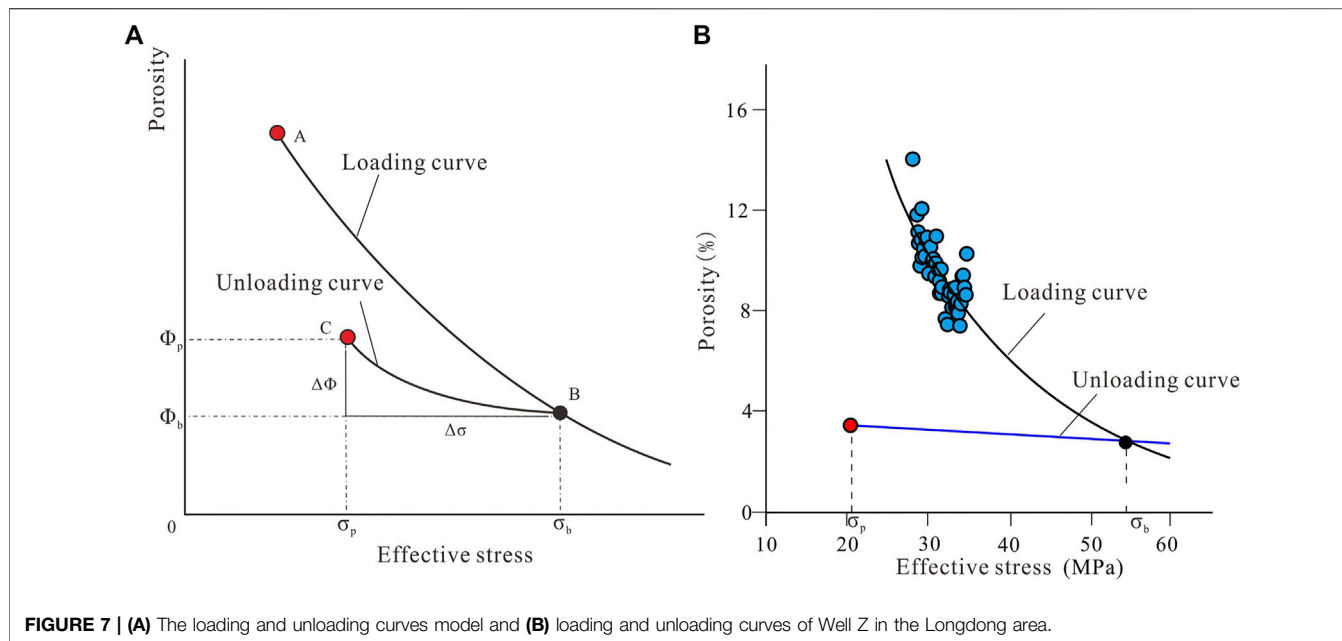
stress reduction during porosity resilience; and ΔP_{dc} is the overpressure caused by under-compaction in the period with the maximum buried depth (see **Figure 6A** for relevant parameters).

Restoration Results of Oil Migration Dynamics During the Main Reservoir-Forming Period

The overpressure of the Chang 8 member in the study area at the end of the Early Cretaceous, when the buried depth reached its maximum, was restored using the method described above, and the overpressure gradient was plotted (**Figure 8**). It was found that the overpressure gradient ranged from <0.5 MPa/m (in the southwest part of the study area) to ˃7.5 MPa/m (in the northeast part of the study area). Specifically, the overpressure gradient was higher in the Baibao Oil Field as well as areas further south (3.0–4.5 MPa/m), and smaller in the area surrounded by the Huachi, Yuele, Qingcheng, and Gucheng oil fields, which is conducive to the stagnation and accumulation of oil. Southward, in the Qingyang, Heshui, and Gucheng oil fields, the overpressure gradient increases and peaks, which is conducive to oil migration and accumulation in ideal traps.

START-UP PRESSURE FOR OIL MIGRATION DURING THE MAIN RESERVOIR-FORMING PERIOD
Relationship Between Start-Up Pressure and Permeability

Research spanning 20 years confirms that tight oil flow in a reservoir typically follows the low-velocity non-Darcy flow

pattern, that is, oil starts to flow at a certain start-up pressure gradient (Zeng et al., 2014). In addition, multiple core flow experiments for tight reservoirs in the Ordos Basin have also suggested that oil could migrate only when the start-up pressure gradient reaches a certain level (Zeng et al., 2014). Based on this, the start-up pressure gradient shows obvious characteristics as the dynamic driver for oil migration in tight reservoirs.

The start-up pressure gradient at which oil enters the transport layer and corresponding permeability data obtained from flow experiments for the Mesozoic tight oil reservoirs in the Ordos Basin were fitted (**Figure 9**) (Wu et al., 2013; Xue and Tian, 2014), and it was found that the start-up pressure has a good correlation with the permeability of samples. The two parameters conform to the power function, with the correlation coefficient of 0.99, expressed as **Eq. 7**:

$$Gp = 0.071K^{1.341} \qquad (7)$$

where Gp is the start-up pressure gradient, MPa/m; and K is the permeability, mD. Using this correlation, the start-up pressure gradient for the formation with permeability data but without flow experiment data could be obtained.

Start-Up Pressure Gradient for Oil Migration During the Main Reservoir-Forming Period

As described above, the start-up pressure gradient was obtained using permeability data and **Eq. 7**. Accordingly, the paleo start-up pressure during tight oil accumulation could also be calculated using the paleo-permeability in the reservoir-forming period. Some scholars have performed diagenesis analyses and determined diagenetic sequence divisions on the basis of sedimentary setting, core observation, and logging data interpretation. They indicated that after the hydrocarbon expulsion peak at the end of the Early
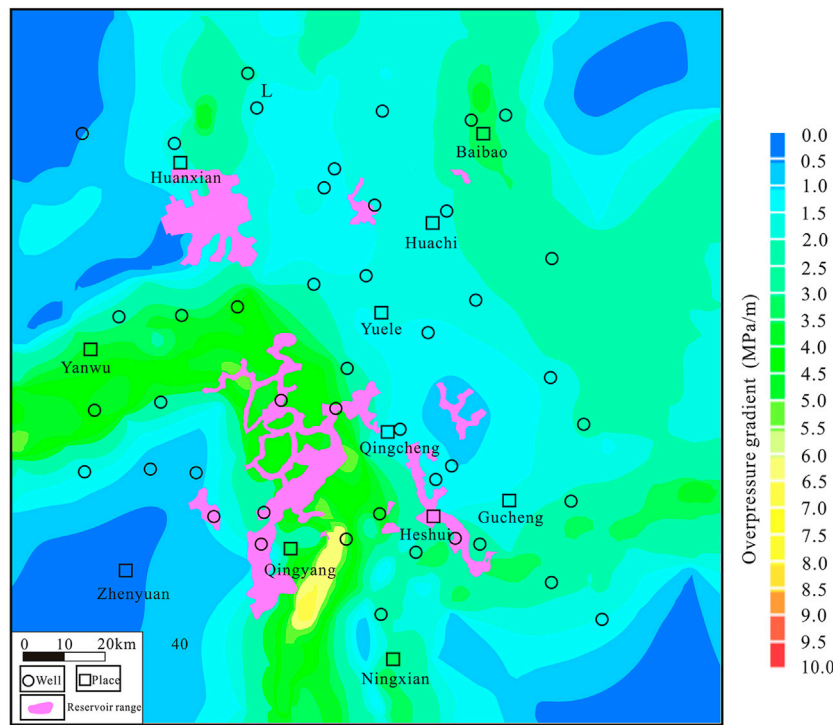
FIGURE 8 | Distribution of the overpressure gradient of the Chang 8 member during the main reservoir-forming period in the Longdong area.
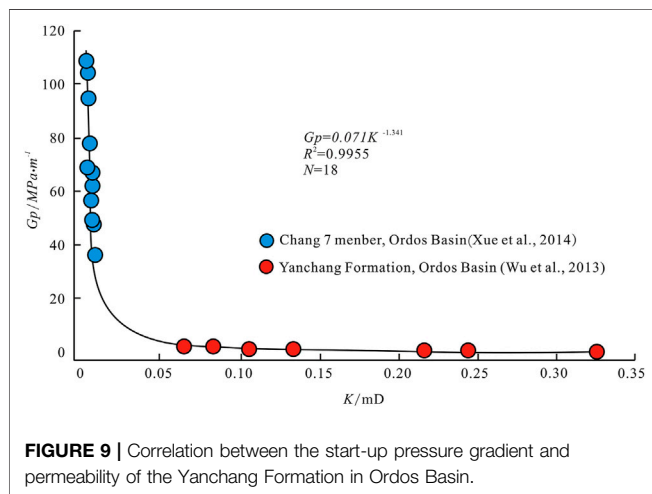
FIGURE 9 | Correlation between the start-up pressure gradient and permeability of the Yanchang Formation in Ordos Basin.

Cretaceous, three types of diagenesis occurred: 1) the replacement of intergranular materials and grain margins by crystalline-connected calcite, 2) the dissolution of matrix and grain margin by highly acidic fluid, and 3) also that by feldspar dissolution. Then, through physical property inversion, they restored the paleo-porosity and paleo-permeability at the maximum buried depth at the end of the Early Cretaceous (Bowers, 1995). From the restored paleo-permeability recovery (Bowers, 1995) and **Eq. 7**, the paleo start-up pressure in this study was determined to be 0.01–0.31 MPa/m. The low start-up pressure gradient (<0.06 MPa/m) was distributed

mainly in N-S orientated segments, located in the central part of the area surrounded by the Zhenyuan, Heshui, and Qingcheng oil fields, as well as in the southern part (especially the center of the distributary channel sand body). Finally, the start-up pressure gradient was high in the eastern part and lowest in the western part (**Figure 10**).

Oil Accumulation Process and Distribution

Fluid potential is an important parameter to determine the potential migration and accumulation direction of oil and gas. Using the restored paleo-structure during the main reservoir-forming period from previous studies (Fan et al., 2013) and the restored paleo-fluid pressure determined in this study, the paleo-fluid potential in the main reservoir-forming period could be calculated from **Eq. 8**, followed by outlining the stream lines with PetroMod software:

$$h_o = z + \frac{P}{\rho_o g} \qquad (8)$$

where h_o is the oil potential; ρ_o is the oil density; z is the height; P is the fluid pressure; and g is the gravitational acceleration.

According to the distribution of oil potential stream lines at the end of the Early Cretaceous (**Figure 11**), it can be concluded that the oil potential is generally higher in the northeast and lower in the southwest. The highest oil potential is located in the northeast of the study area, while the lowest oil potential is located in the Heshui Oil Field in the south and the Zhenyuan Oil Field in the southwest, reflecting a trend of oil migration from northeast to southwest and

FIGURE 10 | Start-up pressure gradient for oil migration in the Chang 8 member during the main reservoir-forming period in the Longdong area.

FIGURE 11 | Oil potential and streamlines for the Chang 8 member during the main reservoir-forming period in the Longdong area.
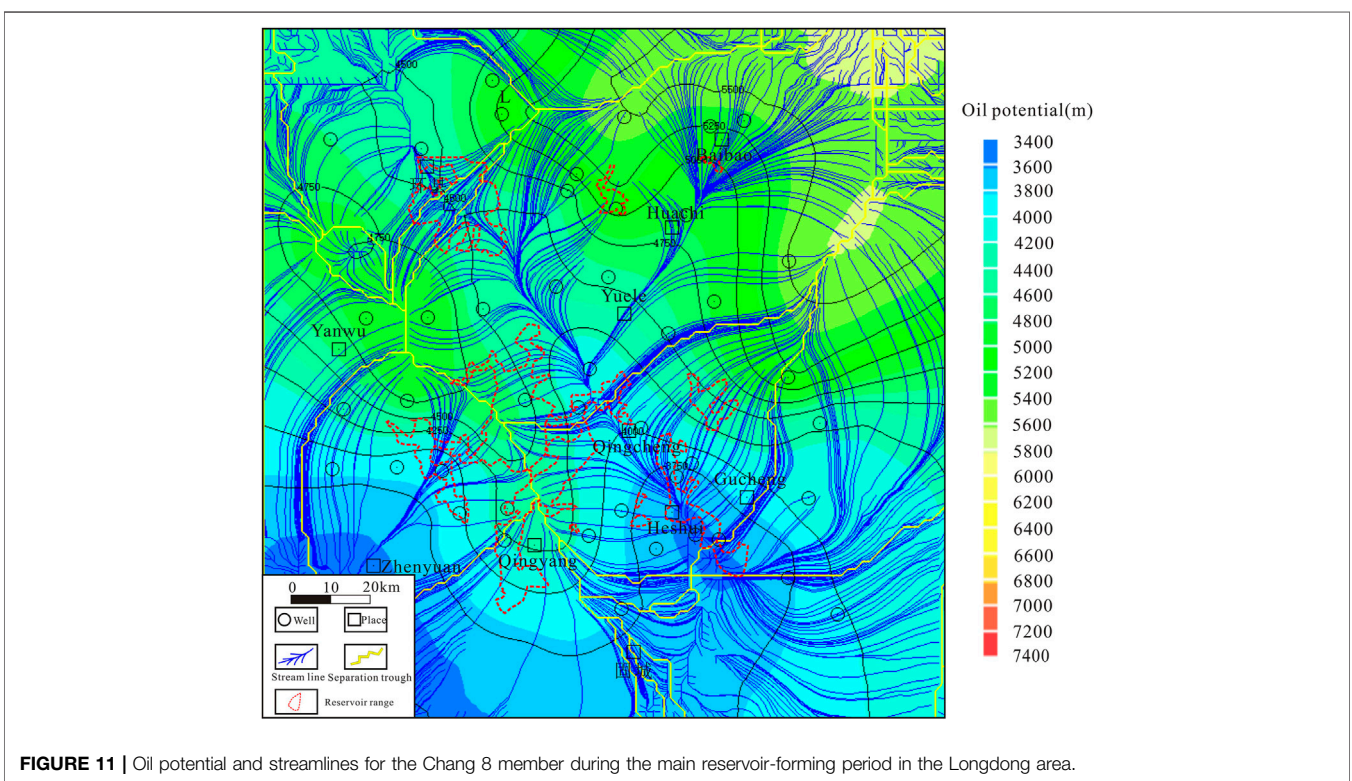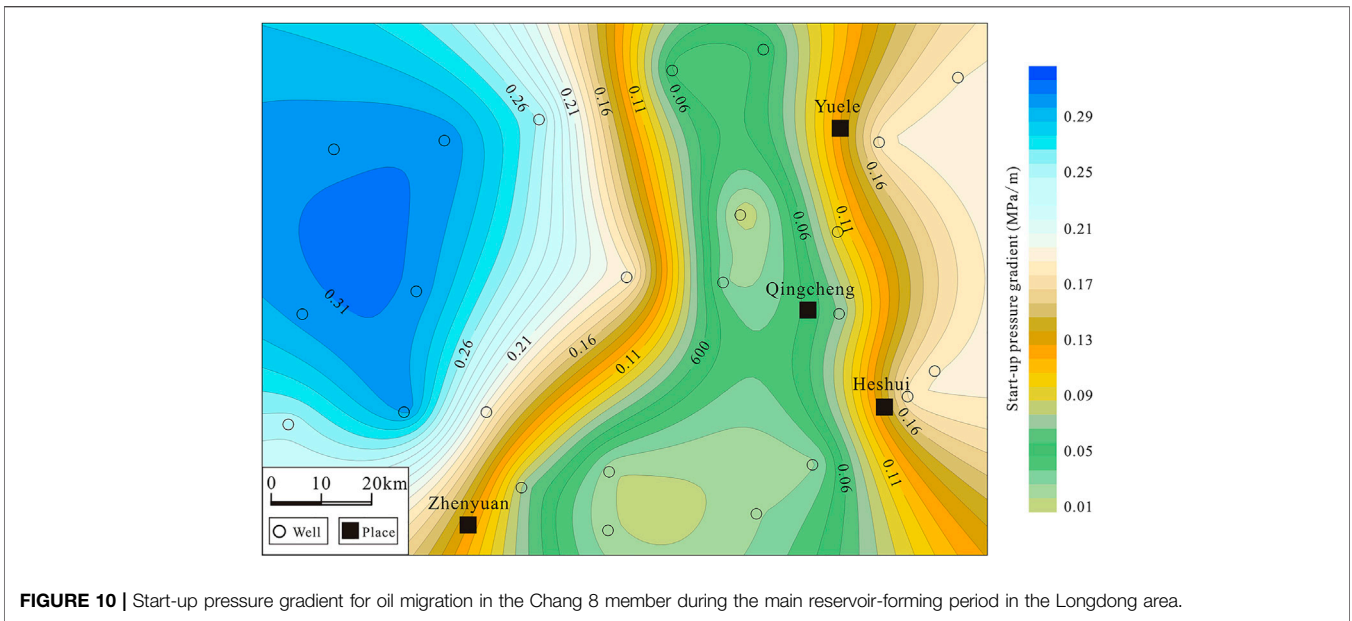
an accumulation in the southwest and south. The stream lines (**Figure 9**) show that oil has migrated from the northeast to the southwest along dominant pathways in the Baibao, Huachi, and Yuele oil fields before accumulating within favorable traps of the Qingcheng, Qingyang, and Heshui oil fields.

Comparison (**Figure 8** and **Figure 10**) indicates that the overpressure gradient in the study area is basically higher than

the start-up pressure gradient during the main reservoir-forming period, and the large difference between the overpressure gradient and start-up pressure gradient falls basically on the dominant migration pathways indicated by the oil potential stream lines (**Figure 10**). Additionally, the reservoir became weakly lipophilic at the end of Early Cretaceous[14], allowing oil to more easily migrate laterally along these areas. The coupling

of migration dynamics and pathway height suggests that oil in the study area mainly migrated from the northeast to the southwest along these areas at the end of the Early Cretaceous and finally accumulated in the large nose-like uplift structure highlighted by the paleo-structure in the southwest (Fan et al., 2013), forming the present Qingcheng, Heshui, and other large oilfields.

After the end of the Early Cretaceous, the Chang 8 member in the north of the Longdong area saw a depleting oil migration for five reasons. First, the subsequent Late Yanshanian structure began to weaken the oil generation capacity of Chang 7 source rocks, which is now very low. Second, the structure rotated counterclockwise and gradually changed from a north-dipping monocline with higher south end and lower north end to a west-dipping monocline with higher east end and lower west end (Fan et al., 2013). Third, the distribution direction of the sand bodies is inconsistent with the trend of monocline. In some areas, sand bodies are distributed almost along the monoclinic trend, with minor structural fluctuation (Fan et al., 2013). Fourth, the physical properties of the reservoir are far inferior to those in the hydrocarbon charging period at the end of the Early Cretaceous (Chen et al., 2006). Fifth, as the abnormal overpressures basically disappeared, the reservoir tended to normal or negative pressure. Therefore, the Huachi Oil Field and other lower abundance reservoirs developed in the oil migration areas in the northeast. In these two stages, the change in intensity of migration dynamics dominated the accumulation and enrichment of tight oil.

CONCLUSION

1) Both the fluid potential and stream lines show that tight oil in the Chang 8 member of the Longdong area tended to migrate from the northeast to the southwest during the main reservoir-forming period, and the overpressure gradient was basically higher than the start-up pressure gradient. According to the potential migration pathways,

oil is now capable of migration from the northeast to the southwest.

2) Following the main reservoir-forming period, due to reservoir compaction-caused diagenesis, and the weakening hydrodynamics and reducing hydrocarbon generation capacity of the source rocks caused by structural uplifting, as well as to reservoir heterogeneity, oil has accumulated near the source rocks but is not as rich as that which accumulated during the reservoir-forming period.

3) During the process of tight oil accumulation, the reservoir was highly heterogeneous in terms of its physical properties, and the change in intensity of migration dynamics dominated the differential accumulation of tight oil (Li and Luo, 2017, Engelder and Behr, 2021, Zhao and Du, 2012).

DATA AVAILABILITY STATEMENT

The original contributions presented in the study are included in the article/Supplementary Material, further inquiries can be directed to the corresponding author.

AUTHOR CONTRIBUTIONS

JY mainly contributed the ideas, research process, and research results of the article. XL mainly contributed some of the original data of the article. WX mainly contributed to the analysis of mudstone compaction law.

FUNDING

REFERENCES

Athy, L. F. (1930). Density, Porosity, and Compaction of Sedimentary Rocks. *AAPG Bull.* 14, 1–24. doi:10.1306/3d93289e-16b1-11d7-8645000102c1865d

Bowers, G. L. (1995). Pore Pressure Estimation from Velocity Data: Accounting for Overpressure Mechanisms besides Undercompaction. *SPE Drilling and Completions* 10, 89–95. doi:10.2118/27488-PA

Chen, H. L., and Tang, X. Y. (1981). A Study of Clay Compaction and Primary Migration of Oil and Gas. *Oil Gas Geology.* 2, 114–122. doi:10.11743/ogg19810203

Chen, Z. K., Wu, Y. S., Luo, X. R., and Chen, R. Y. (2006). Reconstruction of Paleo-Passage System of Chang 8 Formation in Longdong Area, Ordos Basin. *Acta Geologica Sinica* 5, 718–723.

Clarkson, C. R., Jensen, J. L., and Pedemen, P. K. (2011). "Production Analysis of Western Canadian Unconventional Light Oil Plays," in Proceedings of the Canadian Unconventional Resources Conference, Alberta, Canada, 15-17 November 2011. SPE 149005. doi:10.2118/149005-ms

Du, J. H., Li, J. Z., and Guo, B. C. (2016). *Continental Tight Oil in China*. Beijing: Petroleum Industry Press, 2–18.

Engelder, T., and Behr, R.-A. (2021). Skempton's Poroelastic Relaxation: The Mechanism that Accounts for the Distribution of Pore Pressure and Exhumation-Related Fractures in Black Shale of the Appalachian Basin. *Bulletin* 105, 669–694. doi:10.1306/07142019029

Fan, C., and Wang, G. (2021). The Significance of a Piecemeal Geometric Model of Mudstone Compaction: Pinghu Slope, Xihu Depression, Eastern China. *Mar. Pet. Geology.* 131, 105138. doi:10.1016/j.marpetgeo.2021.105138

Fan, C., Wang, Z., Ying, Y., and Liu, J. (2013). Origin and Distribution of Irregular Oil-Water Contacts in Tight Sandstones, Chang 81 Member, Longdong Area, Ordos Basin, China. *Energy Exploration & Exploitation* 31, 667–696. doi:10.1260/0144-5987.31.5.667

Fertl, W. H. (1976). *Abnormal Formation Pressure: Implication to Exploration, Drilling, and Production of Oil and Gas Resources*. Amsterdam: Elsevier. . Available at: http://www.worldoil.com/, 382.

Fertl, W. H., and Timko, D. H. (1972). How Downhole Temperature, Pressure Affect Drilling, Part 3: Overpressure Detection from Wireline Methods. *Word Oil* 8, 36–66.

Fu, J., Deng, X., Wang, Q., Li, J., Qiu, J., Hao, L., et al. (2017). Densification and Hydrocarbon Accumulation of Triassic Yanchang Formation Chang 8 Member, Ordos Basin, NW China: Evidence from Geochemistry and Fluid Inclusions. *Pet. exploration Dev.* 44, 48–57. doi:10.1016/S1876-3804(17)30007-1

Gautier, D. L., Dolton, G. L., Takahashi, K. I., and Varnes, K. L. (1995). *1995 National Assessment of United States Oil and Gas Resources: Results, Methodology, and Supporting Data*. Virginia: US Geological Survey Digital Data Series DDS-30. doi:10.3133/ds30

Han, X. J. (2020). *Forming Process of Underpressure and its Impact on Shale Gas Enrichment, Shan1 Member, southeastern Ordos Basin*. Xi'an, Shaanxi: Northwest University, 1–60. doi:10.27405/d.cnki.gxbdu.2020.000303

Hermanrud, C., Wensaas, L., and Teige, G. M. (1998). "Shale Porosity from Well Logs on Haltenbanken (Offshore mid-Norway) Show No Influence of Overpressuring,". *Abnormal Pressure in Hydrocarbon Environment*. Editors B. E. LAW, G. F. ULMISHEK, and V. I. SLAVIN (Tulsa: American Association of Petroleum Geologists), 70, 65–85. doi:10.1306/M70615C4

Li, C., and Luo, X. R. (2017). Review on Mudstone Chemical Compaction. *J. Earth Sci. Environ.* 39, 761–772. doi:10.3969/j.issn.1672-6561.2017.06.007

Li, D., Li, R., Zhu, Z., Wu, X., Cheng, J., Liu, F., et al. (2017). Origin of Organic Matter and Paleo-Sedimentary Environment Reconstruction of the Triassic Oil Shale in Tongchuan City, Southern Ordos Basin (China). *Fuel* 208, 223–235. doi:10.1016/j.fuel.2017.07.008

Li, D. L., Li, R. X., and Tan, C. Q. (2019). Depositional Conditions and Modeling of Triassic Oil Shale in Southern Ordos Basin Using Geochemical Records. *J. Cent. South Univ.* 26, 3436–3456. SUN:ZNGY.0.2019-12-019. doi:10.1007/s11771-019-4265-6

Li, D., Shi, Q., Mi, N., Xu, Y., Wang, X., and Tao, W. (2020a). The Type, Origin and Preservation of Organic Matter of the fine-grain Sediments in Triassic Yanhe Profile, Ordos Basin, and Their Relation to Paleoenvironment Condition. *J. Pet. Sci. Eng.* 188, 106875. doi:10.1016/j.petrol.2019.106875

Li, J., Zeng, L. B., and Lin, Y. (2020b). Horizontal Fractures of the Cenozoic in Western Qaidam Basin and Their Tectonic Implication. *Oil Gas Geology.* 41, 1222–1232. doi:10.11743/ogg20200620

Liu, Z., Liu, J. J., and Wang, W. (2012). Experimental Analyses on Critical Conditions of Oil Charge for Low-Permeability Sandstones: a Case Study of Xifeng Oilfield. *Ordos Basin. ACTA PETROLEI SINICA* 33, 996–1012. doi:10.7623/syxb201206010

Luo, X. R., Zhang, L. P., and Yang, H. (2010). Oil Accumulation Process in the Low-Permeability Chang 81 Member of Longdong Area, the Ordos Basin. *Oil Gas Geology.* 31, 770–778. doi:10.1016/S1876-3804(11)60008-6

Magara, K. (1978). *Compaction and Fluid Migration, Practical Petroleum Geology.* Amsterdam: Elsevier, 319. doi:10.1016/0037-0738(80)90060-3

Magara, K. (1968). Compaction and Migration of Fluids in Miocene Mudstone, Nagaoka Plain, Japan. *AAPG Bull.* 52, 2466–2501. doi:10.1306/5d25c58d-16c1-11d7-8645000102c1865d

Osborne, M. J., and Swarbrick, R. E. (1997). Mechanisms for Generating Overpressure in Sedimentary basin: a Reevaluation. *AAPG Bull.* 81, 1023–1041. doi:10.1093/ietcom/e90-b.2.425

Ren, Y., and Sun, A. Y. (2005). Porosity Variation in Elastic Deformation of Rock. *Xinjiang Pet. Geology.* 3, 336–338. doi:10.3969/j.issn.1001-3873.2005.03.033

Schmoker, J. W., Beeman, W. R., Obuch, R. C., and Brewton, J. D. (1995). Method for Assessing Continuous-type (Unconventional) Hydrocarbon Accumulations ‖ Gautier, D. L., Dolton, G. L., Takahashi, K. I., et al. *1995 National Assessment of United States Oil and Gas Resources—Results, Methodology, and Supporting Data.* Virginia: US Geological Survey Digital Data Series DDS-30.

Terzaghi, K. (1943). *Theoretical Soil Mechanics*, 510. New York: John Wiley & Sons. doi:10.1002/9780470172766.fmatter

Wang, Z. L., Sun, M. L., and Geng, P. (2003). The Development Features and Formation Mechanisms of Abnormal High Formation Pressure in Southern Junggar Region. *Pet. Exploration Dev.* 30, 32–34. doi:10.3321/j.issn:1000-0747.2003.01.008

Wang, Z., Luo, X., Lei, Y., Zhang, L., Shi, H., Lu, J., et al. (2020). Impact of Detrital Composition and Diagenesis on the Heterogeneity and Quality of Low-Permeability to Tight Sandstone Reservoirs: An Example of the Upper Triassic Yanchang Formation in Southeastern Ordos Basin. *J. Pet. Sci. Eng.* 195, 107596. doi:10.1016/j.petrol.2020.107596

Wang, Z. L., Zhang, L. K., and Shi, L. Z. (2005). Genesis Analysis and Quantitative Evaluation on Abnormal High Fluid Pressure in the Kela-2 Gas Field, Kuqa Depression, Tarim Basin. *Geol. Rev.* 51, 55–63. doi:10.16509/j.georeview.2005.01.009

Wu, K., Luo, L. R., and Kong, Q. F. (2013). Pool-forming Dynamic Characteristics of Extra-low Permeability and Tight Reservoir in Yanchang Formation, Mesozoic Erathem, Ordos basin. *Petrochemical Industry Appl. Pplication* 32, 37–44 doi:10.3969/j.issn.1673-5285.2013.08.010

Xi, K., Cao, Y., Liu, K., Wu, S., Yuan, G., Zhu, R., et al. (2019a). Diagenesis of Tight sandstone Reservoirs in the Upper Triassic Yanchang Formation, Southwestern Ordos Basin, China. *Mar. Pet. Geology.* 99, 548–562. doi:10.1016/j.marpetgeo.2018.10.031

Xi, K., Cao, Y., Liu, K., Wu, S., Yuan, G., Zhu, R., et al. (2019b). Geochemical Constraints on the Origins of Calcite Cements and Their Impacts on Reservoir Heterogeneities: A Case Study on Tight Oil Sandstones of the Upper Triassic Yanchang Formation, Southwestern Ordos Basin, China. *Bulletin* 103, 2447–2485. doi:10.1306/01301918093

Xue, Y. C., and Tian, X. F. (2014). Characteristics of Chang -7 Tight Oil Reservoir, Ordos basin. *Spec. Oil Gas Reservoirs* 21 (3), 111–115. doi:10.3969/j.issn.1006-6535.2014.03.027

Zeng, J. H., Yang, Z. F., and Feng, X. (2014). Study Status and Key Scientific Issue of Tight Reservoir Oil and Gas Accumulation Mechanism. *Adv. Earth Sci.* 29, 651–661. doi:10.11867/j.issn.1001-8166.2014.06.0651

Zhang, W. Zh., Yang, H., and Peng, P. A. (2009). The Influence of Late Triassic Volcanism on the Development of Chang 7 High Grade Hydrocarbon Source Rock in Ordos Bsin. *Geochimica* 38, 573–582. doi:10.19700/j.0379-1726.2009.06.007

Zhao, J. Z., Bai, Y. B., and Cao, Q. (2012). Quasi-continuous Hydrocarbon Accumulation: a New Pattern for Large Tight Sand Oilfields in the Ordos Basin. *Oil Gas Geology.* 33, 811–827. doi:10.11743/ogg20120601

Zhao, J. Z., Fu, J. H., and Cao, Q. (2017). *Tight Oil and Gas Accumulation Theory and Evaluation Technology.* Beijing: Petroleum Industry Press.

Zhao, Y., Wang, Y. B., and Zhong, D. K. (2018). Study on the Relationship between Tight sandstone Reservoir Diagenetic Evolution and Hydrocarbon Reservoirs Filling: A Case from the Yanchang Formation, Ordos Basin. *J. mining Sci. Technol.* 3, 106–118. doi:10.19606/j.cnki.jmst.2018.02.002

Zhao, Z. Z., and Du, J. W. (2012). *Tight Oil and Gas.* Beijing: Petroleum Industry Press, 1–11.

Zou, C. N., Tao, S. Z., and Yuan, X. J. (2009). Global Importance of "Continuous"petroleum Reservoirs: Accumulation, Distribution and Evaluation. *Pet. exploration Dev.* 36, 669–681. doi:10.1016/S1876-3804(10)60001-8

Zou, C. N., Zhu, R. K., Bai, B., Yang, Z., Hou, L. H., Zha, M., et al. (2015). Significance, Geologic Characteristics, Resource Potential and Future Challenges of Tight Oil and Shale Oil. *Bull. Mineralogy, Petrol. Geochem.* 34, 3–17. CNKI:SUN:KYDH.0.2015-01-002. doi:10.3969/j.issn.1007-2802.2015.01.001